IEEE Access
Multidisciplinary | Rapid Review | Open Access Journal

Received March 8, 2021, accepted March 25, 2021, date of publication April 6, 2021, date of current version April 20, 2021.

Digital Object Identifier 10.1109/ACCESS.2021.3071467

Comprehensive Analysis of Time-Domain Hybrid PAM for Data-Rate and Distance Adaptive UWOC System

TAKAHIRO KODAMA[1], (Member, IEEE), MUHAMAD AIZAT BIN AHMAD SANUSI[1], FUMIYA KOBORI[1], TOMOTAKA KIMURA[2], (Member, IEEE), YOSHIAKI INOUE[3], (Member, IEEE), AND MASAHIKO JINNO[1], (Fellow, IEEE)

[1]Faculty of Engineering and Design, Kagawa University, Takamatsu 761-0396, Japan
[2]Faculty of Science and Engineering, Doshisha University, Kyotanabe 610-0394, Japan
[3]Department of Information and Communication Technology, Graduate School of Engineering, Osaka University, Suita 565-0821, Japan

Corresponding author: Takahiro Kodama (kodama.takahiro@kagawa-u.ac.jp)

This work was supported in part by the Grant-in-Aid for Scientific Research (C) of the Japan Society for the Promotion of Science under Grant 18K11282.

ABSTRACT The challenge for next-generation underwater optical wireless communication systems is to develop optical transceivers that can operate with low power consumption by maximizing the transmission capacity according to the transmission distance between transmitters and receivers. This study proposes an underwater wireless optical communication (UWOC) system using an optical transceiver with an optimum transmission rate for the deep sea with near-pure water properties. As a method for actualizing an optical transceiver with an optimum transmission rate in a UWOC system, time-domain hybrid pulse amplitude modulation (PAM) (TDHP) using a transmission rate and distance-adaptive intensity modulation/direct detection optical transceiver is considered. In the TDHP method, variable transmission capacity is actualized while changing the generation ratio of two intensity-modulated signals with different noise immunities in the time domain. Three different color laser diodes (LDs), red, blue, and green are used in an underwater channel transmission transceiver that comprises the LD and a photodiode. The maximum transmission distance while changing the incidence of PAM 2 and PAM 4 signals that calibrate the TDHP in a pure transmission line and how the maximum transmission distance changes when the optical transmitter/receiver spatial optical system is altered from the optimum conditions are clarified based on numerical calculation and simulation. To the best knowledge of the authors, there is no other research on data-rate and distance adaptive UWOC system that applies the TDHP signal with power optimization between two modulation formats.

INDEX TERMS Underwater optical wireless communication, underwater equipment, underwater technology, intensity modulation.

I. INTRODUCTION

Seafloor related research and developments have progressed in areas such as disaster prevention of tsunami and earthquakes, the off-shore oil industry, diver-submarine communications [1], and underwater environment monitoring systems. However, exploring the deep seafloor has been deemed too dangerous for humans as the human body cannot withstand the high pressures associated with the depths. As the complexity and precision of robots has increased and they have proved reliable, they have become entrusted to explore underwater sites. Thus, a reliable means of communications must be established between the operator and machine to give the device instructions. An underwater wireless communications system is valuable since it is the only way to transmit information from the sensors.

For use over a broad range in wireless communications, the standard communication method is to use electromagnetic waves [2]. However, there is a big hurdle to implement this type of communication system underwater. Since electromagnetic waves are attenuated easily underwater, alternatives such as acoustic waves have became popular due to their low attenuation and long-range transmission capability. The main problem with acoustic waves is the narrow bandwidth,

The associate editor coordinating the review of this manuscript and approving it for publication was Maged Abdullah Esmail.

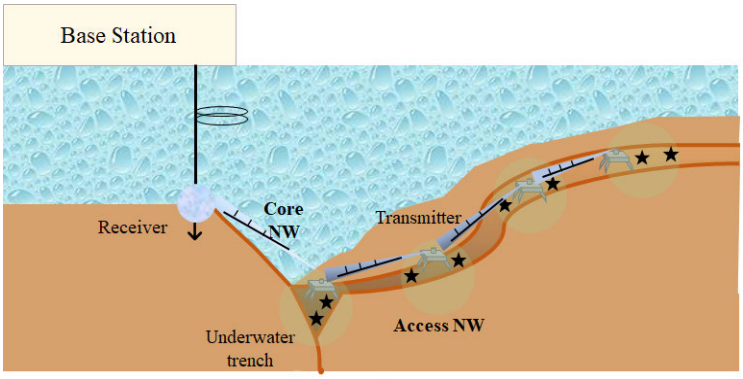

FIGURE 1. Overall structure of UWOC system.

which leads to high latency and high-power consumption. There are efforts to use other types of waves such as very low-frequency radio waves used by naval submarines to penetrate the depths to the seafloor. The low frequency causes natural background noise to increase and requires more power to overcome the noise. Due to this, acoustic waves are not reliable for high-speed underwater transmission. These problems have hindered large-scale use of underwater devices. Due to the few options for reliable underwater transmission, underwater-based machine development has stagnated for many years.

The one of major problem for the current onshore earthquake prediction system is the delay in earthquake prediction. Recent studies have shown that earthquake prediction techniques using seafloor observations are more accurate than the traditional onshore earthquake prediction technique that is still in use today [3]. The seafloor observation method can be developed into a higher-performance system by arranging many underwater Internet-of-Things (IoT) sensors on the seafloor. Underwater wireless optical communication (UWOC) system has been expected to establish a high-capacity underwater communication system [4], [5]. However, to operate this type of system efficiently, an UWOC system must be constructed in advance [6]. Therefore, research and development on optical transceivers for UWOC systems are required [7].

Fig. 1 shows the overall structure of the UWOC system. The previously proposed UWOC system consists of three main components [4]: the access network, core network, and wired-wireless integration. This investigation focuses on the transceiver specifications for a short-reach underwater channel. For the transmitter, we use a light-emitting diode (LED) [8] and laser diode (LD) [9].

From the view of modulation optimization for the transmission channel, signal-to-noise ratio (SNR) adaptive time-domain hybrid pulse amplitude modulation (PAM) (TDHP) [10]–[13] that uses two-level PAM (PAM 2) [14] and four-level PAM (PAM 4) signals together [15], [16] at the transceiver was proposed for optical fiber communication and indoor wireless optical communication systems to address the changes in SNR. The TDHP method is advantageous because it maximizes the transmission capacity by flexibly setting two types of PAM-M signal ratios to the received SNR, which changes according to the water turbidity and transmission distance. The TDHP method can also change only the operation mode in digital signal processing (DSP), and does not require optical and radio frequency (RF) analog components. Since the operation of the TDHP method can be controlled using only software, it is easy to implement and is system scalable. In UWOC transmission, TDHP uses a single carrier that can be received by lowering the signal rate while maintaining the received SNR symbol rate, which is difficult with a pure PAM 4 signal.

As opposed to other research, we use the TDHP method to transmit data in an underwater channel using the UWOC system. Past research mainly used the orthogonal frequency-division multiplexing (OFDM) method for underwater and indoor transmission [17], [18]. The TDHP signal has a lower peak-to-average power ratio (PAPR) than the OFDM signal. The input voltage received by the transmitter driver amplifier is limited, so the average power transmitted from the LD is considerable.

In this paper, we consider a TDHP-based optical transceiver comprising an LD that is included in the core and access networks to maximize the transmission rate and distance corresponding to the received SNR. The SNR changes according to the transmission distance and water turbidity when the transmission distance between each wireless terminal is different in the UWOC system.

As a contribution to the research field of Gigabit-class high-speed underwater optical wireless communication system, the transmission capacity and transmission distance are maximized according to the transmission environment by simply changing two parameters of our proposed TDHP by software control in the transceiver. The novel point is to introduce a flexible modulation for a single carrier system used in the transceiver. The required transmission capacity can be controlled by changing the generation ratio of PAM2 and PAM4 format, the first parameters. By changing the average power of PAM2 and PAM4, which are the second parameters, the maximum transmission distance can be achieved with respect to the set transmission capacity. In this modulation

TABLE 1. Water characteristics.

Water Type	Chlorophyll Concentration	Gelbstoff Concentration	Plankton Concentration	Optimum Wavelength
Pure water Seafloor water	Low	Low	Low	450-500nm (blue-green)
Shallow sea water	High	High	High	520-570 nm (yellow-green)
Dirty water	Very high	Very high	Very high	520-570 nm (yellow-green)

method for pure water channel condition, the effect of optimizing the optical system on typical three visible light RGB colors is also verified by numerical analysis and Monte-Carlo simulation for the first time.

This paper is organized as follows. In Section II, the principle behind submarine optical wireless communication is explained. In Section III, we make the simulation model of TDHP and the calculation model of the maximum transmission distance. In Section IV, we show two results: noise tolerance of TDHP signals and transmission characteristics in seafloor transmission channel. In Section V, we discuss the case of misalignment and fine adjustments to the optical system setup.

II. PRINCIPLE BEHIND SEAFLOOR OPTICAL WIRELESS COMMUNICATIONS

A. PROPERTIES OF SEAFLOOR

The transmitter transmits the TDHP signal via an underwater channel, so the underwater channel properties and their effect on the TDHP signal should be considered.

The Beer-Lambert (BL) law concerns the absorption of radiant energy by an absorbing medium and in this case, water particles are used to evaluate the optical properties of the seafloor [19]. One of the main factors affecting signal deterioration in the UWOC system is signal attenuation due to the absorption and scattering effects underwater. The power delivered can be calculated by using the BL law as

$$P_d = P_0 \exp(-K_T d) \tag{1}$$

where P_0 is the transmitted power, K_T is the beam attenuation coefficient, and d is the distance between the transmitter and the receiver. Beam attenuation coefficient K_T can be calculated using

$$K_T = K_A + K_S \tag{2}$$

where K_A is the absorption rate coefficient and K_S is the scattering coefficient. Absorption coefficient K_A is further calculated using

$$K_A = K_{A0} + Ta \tag{3}$$

Here, K_{A0} is the non-temperature-dependent absorption rate coefficient, T is the water temperature, and a is the temperature coefficient. This equation shows that the signal absorption effect depends on the temperature of the underwater channel.

Based on (1), we show that the BL law only considers attenuation due to two factors: absorption and scattering. It does not assume any collection of scattered light that contributes to the received power. The reason for this is that some of the scattered light will be collected by the receiver [20]. The scattered light will affect lower received power caused by the significant scattering effect of highly turbid water.

The attenuation rate depends on the turbidity of the water, i.e., the murkier the water, the higher the attenuation rate. Table 1 gives the chlorophyll concentration, Gelbstoff concentration, plankton concentration, and the optimum wavelength of three water types: pure water, seawater, and dirty water [21]. Chlorophyll is a green pigment found in algae that allows it to absorb energy from sunlight. Gelbstoff is dissolved yellow organic matter that causes the seawater to appear green, yellow-green, or brown [22]. The concentrations of chlorophyll, Gelbstoff, and plankton reflect the turbidity of the water. The properties of the water types are investigated to reflect the common real-world underwater channel of the UWOC system. Based on Table 1, the chlorophyll concentration, Gelbstoff concentration, and plankton concentration are the lowest for pure water, followed by seawater, and dirty water. The optimum wavelength is the highest for dirty water and seawater at 520-570 nm, while pure water has the lowest optimum wavelength at 450-500 nm. These results suggest that the higher the water turbidity, the higher the optimum wavelength of the LD/LED needed to overcome the attenuation effect.

To understand further the optical properties of the seafloor, we reviewed previous research on the optical properties of deep-sea sites in the Mediterranean conducted by the Neutrino Mediterranean Observatory (NEMO) project in 1999 using a neutrino telescope deployed on the seafloor off the coast of Italy [23]. The absorption coefficient and the attenuation coefficient in the seas around Italy at various water depths were calculated for three years. This study concluded that pure water conditions follow the Smith and Baker model of pure water conditions [24]. Also, the passage of time has little effect on the optical properties of the seafloor. Thus, long-term usage of the UWOC system is viable.

B. SPATIAL OPTICAL CONFIGURATION

This section describes the functions, properties, and factors affecting the effectiveness of the LD and photodetector (PD) for the UWOC system. Generally, the Spatial Optical System (SOS) factors are transmission power P_t, beam attenuation coefficient K, and transmission length d. Fig. 2 shows that the transceiver layout consists of an LD and PD [25].

TABLE 2. SNR tolerance and number of bits per symbol for PAM signals.

	Pure PAM2	TDHP	Pure PAM4
SNR tolerance	High	Middle	Low
Number of bits per symbol	1 (Low)	1+p (Middle)	2 (High)

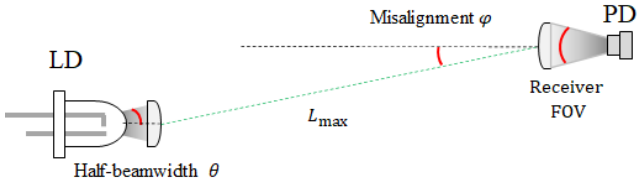

FIGURE 2. Structure of optical components.

An LD is a module that converts an electrical signal into an optical intensity signal to be transmitted via the underwater channel. The factors affecting the LD are the half-angle of the transmitter beamwidth, θ, and the Noise Equivalent Power (NEP) [26]. The NEP is a standard metric that quantifies the PD sensitivity or the power generated by a noise source.

A PD is a module that receives and converts the transmitted optical intensity signal from an LD into an electric signal again. The factors affecting the PD are receiver aperture diameter D, the receiver field-of-view (FOV), and angle misalignment between the line-of-sight (LOS) and the optical axis of the receiver.

C. TIME-DOMAIN HYBRID PAM SIGNAL

The TDHP signal comprises conventional PAM 2 and PAM 4 signals [27]. Table 2 gives the SNR tolerance and the number of bits per symbol for pure water PAM 2 (Pure PAM 2), TDHP, and pure PAM 4 signals. The pure PAM 2 signal achieves a high SNR tolerance [28], but it has a lower data rate of 1 bit per symbol. In contrast, the pure PAM 4 signal has a low SNR tolerance and a higher data rate of 2 bits per symbol [29], [30]. On the other hand, the TDHP signal SNR tolerance and the number of bits per symbol is between that for pure PAM 2 and pure PAM 4.

Parameters of PAM 4 generation ratio p and power control factor q are used to optimize the TDHP signal. The equation below defines the effects of the p and q overall performance of the TDHP bit error rate (BER).

$$\mathrm{BER}_{\mathrm{PAM2}} = \frac{1}{2}\mathrm{erfc}\left(\sqrt{\frac{1}{2}\mathrm{SNR}\,(1-q)}\right) \tag{4}$$

$$\mathrm{BER}_{\mathrm{PAM4}} = \frac{3}{8}\mathrm{erfc}\left(\sqrt{\frac{1}{14}\mathrm{SNR}\,(1+q)}\right) \tag{5}$$

$$\mathrm{BER}_{\mathrm{TDHP}} = p\mathrm{BER}_{\mathrm{PAM4}} + (1-p)\,\mathrm{BER}_{\mathrm{PAM2}} \tag{6}$$

where $\mathrm{BER}_{\mathrm{PAM2}}$, $\mathrm{BER}_{\mathrm{PAM4}}$, and $\mathrm{BER}_{\mathrm{TDHP}}$ are the BERs for the PAM 2, PAM 4, and TDHP signals, respectively. In (6), p is used to control the PAM 2 and PAM 4 occurrence ratio inside TDHP so that the TDHP has an optimized data rate [31]. The p parameter controls the $\mathrm{BER}_{\mathrm{PAM2}}$ and $\mathrm{BER}_{\mathrm{PAM4}}$ inside the transmission distance of pure water. By increasing p, the PAM 4 BER will increase while that for PAM 2 will decrease. Since the PAM 4 signal has a higher bit rate, the overall rate will increase. On the other hand, q is used to control both the signal power of PAM 2 and PAM 4. The q parameter controls the SNR for PAM 2 and PAM 4. As shown in (4) and (5), by increasing q, the PAM 4 power ratio will increase while that for PAM 2 will decrease. This leads to better performance for PAM 4 at the cost of worse performance for PAM 2. However, the overall TDHP performance will be better. The p and q parameters must be adjusted according to the transmission distance and water quality to maintain as high an SNR tolerance as possible while achieving the optimized number of bits per symbol.

III. CONFIGURATION

A. SIMULATION CONFIGURATION FOR TDHP SIGNAL

Fig. 3 shows the simulation configuration for the optical transceiver for the non-return zero (NRZ) TDHP system under pure water conditions. The two types of modulation, the NRZ PAM 2 and PAM 4 signal ratio and power ratio are configured using the p and q parameters.

On the transmitter side, the TDHP signal is generated. The TDHP symbol is modulated at the mapper. The TDHP signal has low power, so for the LD to transmit the signal the driver amplifier (DA) increases the TDHP signal power according to the LD transmission power configuration. Subsequently, the TDHP signal is transferred to the LD. The optically modulated TDHP signal is transmitted to the receiver via the pure water channel.

On the receiver side, the PD detects the TDHP signal. The received TDHP signal power is low due to the underwater transmission, so a transimpedance amplifier (TIA) increases the TDHP signal power. Subsequently, the received TDHP signal is demodulated at the demapper. Then, the TDHP bit sequence is used to calculate the SNR with respect to the BER. Based on the results, an SNR-BER graph is generated. A lower BER means high TDHP performance, while a higher BER means low TDHP performance. The TDHP performance improves by adjusting the p and q parameters.

The simulation parameters are shown in Table 3. There are two types of generated signals: PAM 2 and PAM 4. We combine these signals to create a TDHP signal. The p and q parameters control the signal ratio and power ratio of the PAM 2 and PAM 4 signals to optimize the TDHP signal. The p parameter controls the NRZ and PAM 4 signal ratio. By increasing p, the PAM 4 signal ratio increases, and the PAM 2 signal ratio decreases. Overall, the TDHP signal data rate increases. The q parameter controls the power ratio between the PAM 2 and PAM 4 signals. Increasing q increases the PAM 4 signal power while the PAM 2 signal power decreases simultaneously.

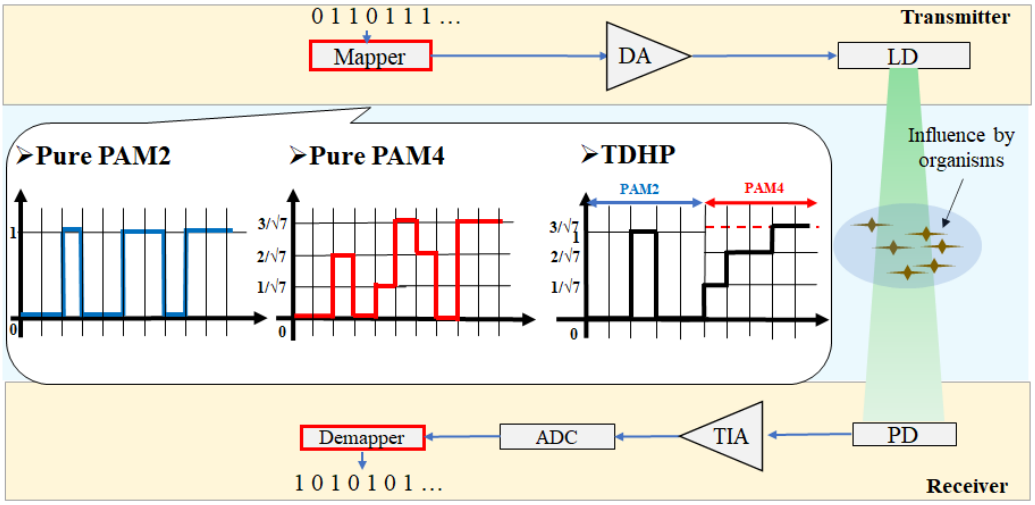

FIGURE 3. Block diagram of simulation.

TABLE 3. Parameters for numerical calculation.

Parameter	Symbol	Unit	Value
Transmission power	P_t	Watt	0.5
Noise power	P_n	Watt	2×10^{-6}
Beam attenuation coefficient	K	1/Meter	Red light (650 [nm]): 3×10^{-1} Green light (550 [nm]): 7×10^{-2} Blue light (450 [nm]): 2×10^{-2}
Receiver aperture diameter	D	Meter	0.2
Focal length	F	Meter	0.6
Angle misalignment between the optical axis of the receiver and the line-of-sight between Tx and Rx	φ	Degree	10
Half-angle Tx beamwidth	θ	Degree	10
Receiver field-of-view	FOV	Degree	10
Noise equivalent power	NEP	Watt / √Hz	0.4×10^{-12}
Transmission bandwidth	BW	Hz	1×10^{9}

B. CALCULATION OF MAXIMUM TRANSMISSION LENGTH

We propose the UWOC system structure comprising an LD and PD [32]. The LD acts as the transmitter that converts the electronic signal into an optical intensity signal. Meanwhile, the PD is a receiver that converts the transmitted light signal into an electronic signal again. These two components are crucial to the UWOC system to send the TDHP signals through the underwater channel.

On the transmitter side, the ratio of PAM 2 and PAM 4 of the TDHP signal is adjusted, and then the symbol pattern of the TDHP signal is mapped at the symbol mapper. The TDHP signal is generated and then converted to an analog electrical signal in the digital-to-analog converter. Subsequently, the TDHP signal is launched into the input of the LD. Here, the TDHP signal is optically modulated to enable transmission using optical light. The transmitted TDHP signal then reaches the receiver via the underwater channel.

On the receiver side, the PD detects the TDHP signal. We note here that signal deterioration may occur during the LD-PD signal transmission. Signal deterioration is due to two main factors: transmission distance and water turbidity. In terms of water turbidity, not only water molecules but also the influence of organisms should be taken into the calculations to simulate real-world surroundings. The TDHP signal is converted into a digital signal using an analog-to-digital converter (ADC). From here, the digital TDHP signal is reconstituted into original bit sequence via demapping.

Three types of LDs, red light, green light, and blue light, are achieved by changing beam attenuation coefficient K. The SNR equation used in the simulation is

$$\mathrm{SNR} = \frac{P_t D^2 \cos\varphi}{4\left(\tan^2\theta\right) P_n} \times \frac{e^{-KL_{\max}}}{L_{\max}^2} \tag{7}$$

where P_t is the transmission power, D is the receiver aperture, φ is the angle misalignment between the optical axis of the receiver and the LOS of the transmitter and the receiver, K is the beam attenuation coefficient, $L_{\max}$ is the maximum transmission distance, θ is the half-angle transmitter beamwidth,

and P_n is the noise power. We explain the details of parameter θ in Section II.B. For noise power P_n, we assume that the power of the received optical signal is so low that the contribution of shot noise to P_n is negligible. Therefore, we use a constant value that constitutes thermal noise only. Aperture D can be calculated using

$$D = 2F \tan(\text{FOV}) \tag{8}$$

where FOV is the receiver field-of-view, and F is the receiver focal length [33], [34]. In the simulations all parameters can be controlled. However, to obtain the value of $L_{\max}$, the SNR equation must be recalculated as

$$e^{KL_{\max}} \cdot L_{\max}^2 = \frac{P_t D^2 \cos\varphi}{4\left(\tan^2\theta\right) P_n \text{SNR}} \tag{9}$$

Subsequently, beam attenuation coefficient K, half-beamwidth θ, misalignment φ, and the FOV are used as controlled parameters.

We use the LD to transmit TDHP signals because it can support a high transmission capacity of approximately 1 Gsymbol/s. In addition, LD lights are energy-efficient and yield no electromagnetic interference making the LD light a prime choice for the UWOC system. The three LD light colors of red, green, and blue are studied to determine the maximum transmission distance for each color. In terms of angle deviation, the default angle is set to 10° being the variable in the simulation.

Here, only simulations were performed. The beam attenuation coefficient K is taken from the Smith and Baker model. While the light intensity is kept constant, we measure the maximum transmission distance of red, green, and blue according to half-beamwidth θ, misalignment φ, and the receiver FOV. Other remaining parameters are only for monitoring variables, so no simulations are conducted in which those parameters are varied. To operate the TDHP method in real-time, the p parameter is adaptively changed while constantly measuring based on the transmission distance $L_{\max}$ and misalignment angle φ measurement between transmitters and receivers by ultrasonic communication and the surrounding turbidity sensor's information related to the beam attenuation coefficient K. Unlike the OFDM method, the TDHP method does not need to adaptively monitor each frequency band's transmission characteristics to which subcarriers are assigned.

IV. RESULTS

A. NOISE TOLERANCE PERFORMANCE

To obtain an optimized TDHP signal, we measure and select the lowest forward error correction (FEC) limit with a threshold of BER $= 3.4 \times 10^{-3}$ for TDHP for each power ratio when the signal ratio is kept constant. In this way, we can obtain the optimum TDHP signal for each p and q range from 0 to 1 in increments of 0.1 for each. When the PAM 4 ratio p is equal to 0 or 1, the generated signal comprises pure PAM 2 and pure PAM 4 signals. Thus, the q parameter is not considered.

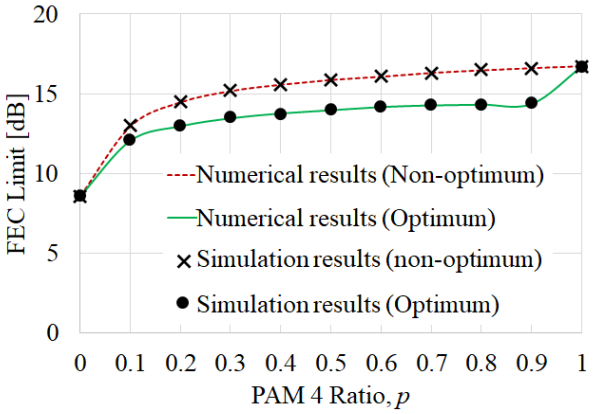

FIGURE 4. FEC limit of non-optimum and optimum TDHP signals according to PAM 4 ratio *p*.

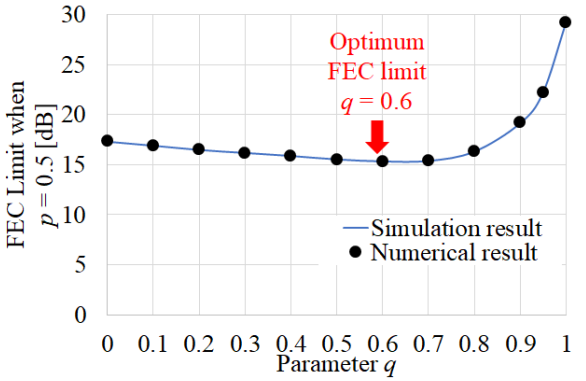

FIGURE 5. FEC limit of TDHP signal for parameter *q* when $p = 0.5$.

Fig. 4 shows the FEC limit of the optimum and non-optimum TDHP signals for each PAM 4 ratio p. The figure shows that when PAM 4 ratio p is 0 or 1, the optimum and non-optimum FEC limits are the same. However, when $p = 0.1$ to 0.9, the FEC limit of the optimum TDHP is lower than the non-optimum TDHP with a difference of approximately -2 dB. We use two methods to verify the FEC limit value: numerical calculation and Monte Carlo simulation. This Monte Carlo simulation used MATLAB software.

As an example, Fig. 5 shows the FEC limit for each q parameter when the p parameter is fixed to 0.5. The results show that as q increases, the FEC limit decreases until 0.6, which is the optimum FEC limit for $p = 0.5$. After the optimum point, the FEC limit increases. The calculation is performed for $q = 0.1$ to 0.9.

From these results, we can see that the difference between the optimum and non-optimum results is approximately 2 dB. For the optimum TDHP, when the PAM 4 ratio p is between 0.1 to 0.9, the lowest FEC limit is selected to obtain the optimum signal. For this reason excellent performance can be preserved even as the low noise tolerance PAM 4 ratio increases.

For the TDHP signal, the SNR is controlled by the q parameter, while the p parameter controls the BER. From these results, we conclude that when the p parameter

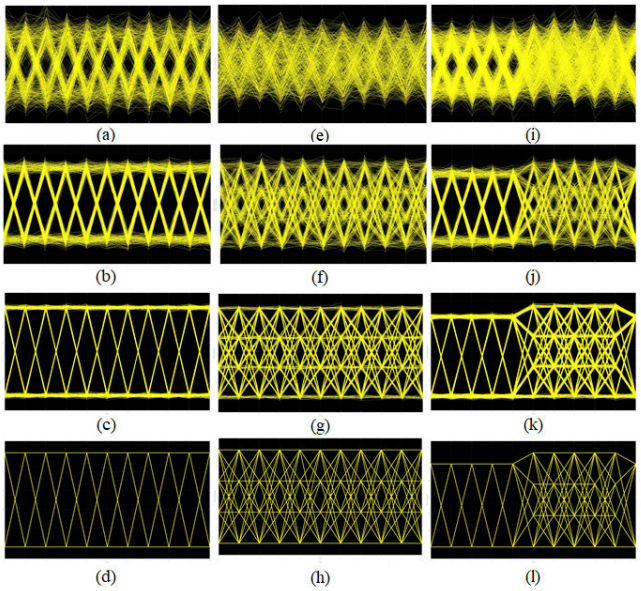

FIGURE 6. Eye diagram (a) Pure PAM 2 at SNR = 10 dB, (b) Pure PAM 2 at SNR = 20 dB, (c) Pure PAM 2 at SNR = 30 dB, (d) Pure PAM 2 at noise-free, (e) Pure PAM 4 at SNR = 10 dB, (f) Pure PAM 4 at SNR = 20 dB, (g) Pure PAM 4 at SNR = 30 dB, (h) Pure PAM 4 at noise-free, (i) TDHP ($p = 0.5$, $q = 0$) at SNR = 10 dB, (j) TDHP ($p = 0.5$, $q = 0$) at SNR = 20 dB, (k) TDHP ($p = 0.5$, $q = 0$) at SNR = 30 dB, (l) TDHP ($p = 0.5$, $q = 0$) at noise-free.

increases, the noise tolerance properties of the TDHP signals decreases. However, by using the optimal peak q parameter, the performance of the TDHP signal improves.

Figs. 6(a-d), 6(e-h), 6(i-l) show the eye diagrams for pure PAM 2, pure PAM 4, and TDHP ($p = 0.5, q = 0$), respectively, for SNR = 10, 20, 30, and noise-free conditions. These figures show that a higher SNR reduces the distortion of the eye diagram. They also show that increasing the SNR improves the overall performance for the pure PAM 2, pure PAM 4, and TDHP signal. When the eye diagram of TDHP when p is set to 0.5 and $q = 0$, the PAM 2 and PAM 4 ratios are the same. The eye diagrams for TDHP show that it has an equal amount of PAM 2 and PAM 4 eye diagrams. From Fig. 6 (i-l), we can confirm that under the condition of $p = 0.5$, PAM 4 is more susceptible to noise than PAM 2 and the eye-opening is smaller, so optimization by adjusting the q parameter is necessary.

B. SEAFLOOR TRANSMISSION PERFORMANCE

We determine the effect of PAM 4 ratio p on maximum transmission distance $L_{\max}$ for the red, green, and blue LDs. Fig. 7 shows the relation between PAM 4 ratio p and maximum transmission distance $L_{\max}$ of the optimum and non-optimum red, green, and blue lights.

The blue light has the longest $L_{\max}$, followed by the green light. The red light has the shortest $L_{\max}$. The red, green, and blue light wavelengths are 650 nm, 550 nm and 450 nm, respectively. The same wavelength is used in both the optimal and non-optimal cases. The results suggest that $L_{\max}$ is affected by the wavelength of the color. From the relation of the light color wavelength and $L_{\max}$, we conclude that the shorter the light color wavelength, the longer $L_{\max}$.

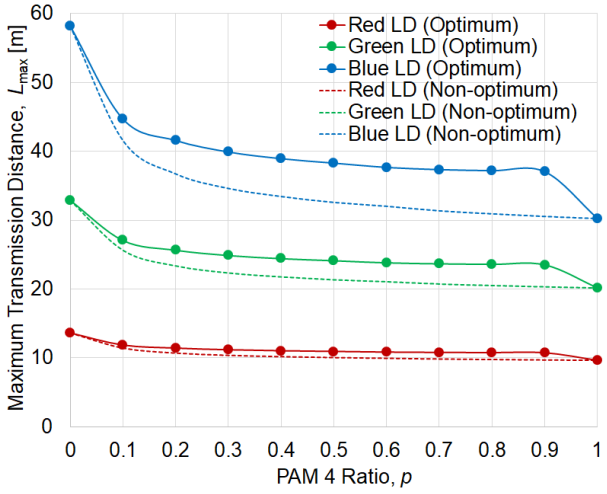

FIGURE 7. Comparison of PAM 4 ratio p and maximum transmission distance $L_{\max}$.

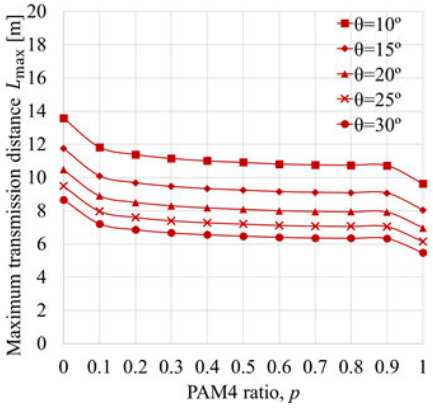

FIGURE 8. Effect of half-beamwidth θ on maximum transmission distance $L_{\max}$ for red LD.

Then, we compare the non-optimum $L_{\max}$ value with the optimum $L_{\max}$ value to see the overall improvement in $L_{\max}$. From Fig. 7, the $L_{\max}$ improvement in the red, blue, and green LDs are approximately 1 m, 2.5 m, and 5 m respectively. The maximum transmission distance improvement is for $p = 0.9$, which is obtained by reducing the required SNR at the FEC limit by optimizing q, which adjusts the average power of PAM 2 and PAM 4, as shown in Fig. 4. The blue light exhibits the best improvements, followed by the green light. The red light exhibits the lowest improvements. These results suggest that the ranges affect the total distance. We conclude that the wider the difference in the highest and lowest $L_{\max}$ values, the easier it is for $L_{\max}$ to deteriorate.

V. DISCUSSION

A. EFFECT OF HALF-ANGLE TRANSMISSION BEAMWIDTH

In this sub-section, we evaluate the effects of half-beamwidth θ towards the overall transmission distance for the optimum q value.

Fig. 8 shows the effect of half-beamwidth θ on maximum transmission distance $L_{\max}$ using the red LD.

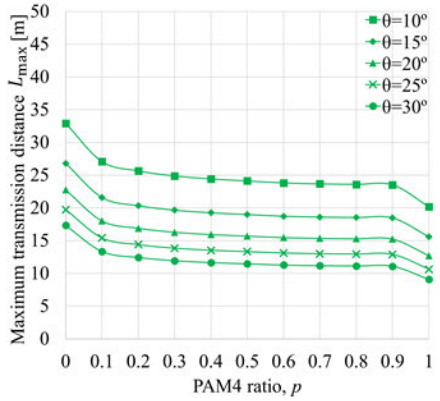

FIGURE 9. Effect on half-beamwidth θ on maximum transmission distance L_{max} for green LD.

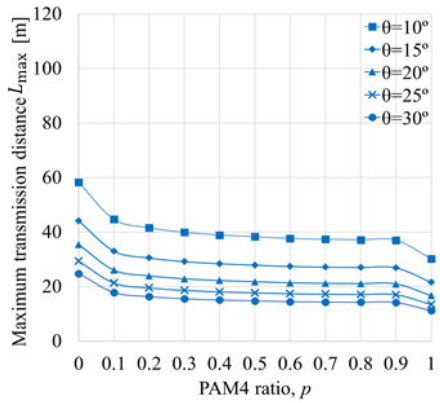

FIGURE 10. Effect on half-beamwidth θ on maximum transmission distance L_{max} for blue LD.

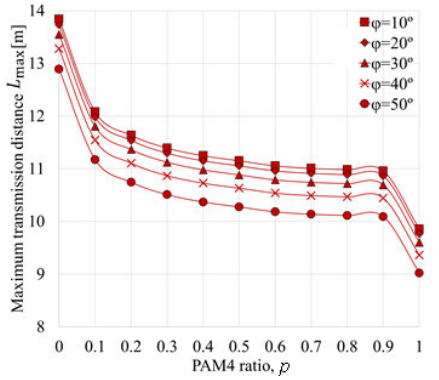

FIGURE 11. Effect of misalignment φ on maximum transmission distance L_{max} for red LD.

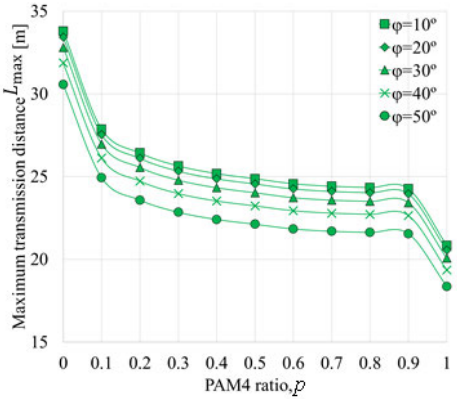

FIGURE 12. Effect of misalignment φ on maximum transmission distance L_{max} for green LD.

When comparing L_{max} values for the optimum and non-optimum transmissions, the improvements are the lowest at approximately 1 m. A moderate improvement is observed from 14 to 10 m. As p increases, L_{max} decreases, with the lowest L_{max} value occurring when $\theta = 30°$, ranging from 8.5 to 5.8 m.

Fig. 9 shows the effect of half-beamwidth θ on maximum transmission distance L_{max} using the green LD. When comparing L_{max} values for the optimum and non-optimum transmissions, the best improvements occur at approximately 2 m. When the initial half-beamwidth $\theta = 10°$ is used, the green LD L_{max} value is from 33 to 20 m. As p increases, L_{max} decreases, with the lowest L_{max} value occurring when $\theta = 30°$, ranging from 17.5 to 9 m. Fig. 10 shows the effect of half-beamwidth θ on maximum transmission distance L_{max} using the blue LD. When comparing the L_{max} values for the optimum and non-optimum transmissions, the highest improvements occur at approximately 4 m. When the initial half-beamwidth $\theta = 10°$ is used, the blue LD L_{max} value is from 58 to 30 m. As p increases, L_{max} decreases, with the lowest L_{max} vale occurring when $\theta = 30°$, ranging from 25 to 11 m.

The results show that beamwidth θ significantly affects L_{max}. As half-beamwidth θ increases, L_{max} decreases. The results indicate that to improve L_{max}, beamwidth θ must be narrowed. As transmitter half-beamwidth θ increases, the beam intensity decreases leading to a lower L_{max} value.

B. ANGLE MISALIGNMENT BETWEEN RECEIVER OPTICAL AXIS AND LOS

A change in misalignment φ could affect the transmission distance. In the case of the optimum q and $\varphi = 0°$, the Tx-Rx LOS and the receiver optical axis are equal. Therefore, the maximum transmission distance is the highest.

The effects of the receiver FOV angle towards L_{max} are evaluated. The L_{max} value ranges from 5° to 25° in increments of 5° for each measurement. For this simulation, the value of φ is 5°, 10°, 15°, 20°, and 25°.

Fig. 11 shows the effect of misalignment φ on maximum transmission distance L_{max} using the red LD. When comparing the L_{max} values for the optimum and non-optimum transmissions, the lowest improvements occur at approximately 0.8 m. When the initial misalignment $\varphi = 10°$ is used, the red LD L_{max} value is 11 to 14 m. As p increases, L_{max} decreases with the lowest L_{max} value occurring when $\varphi = 50°$ ranging from 9 to 13 m.

Fig. 12 shows the effect of misalignment φ on maximum transmission distance L_{max} using the green LD. When comparing the L_{max} values for the optimum and non-optimum transmissions, the best improvements occur at

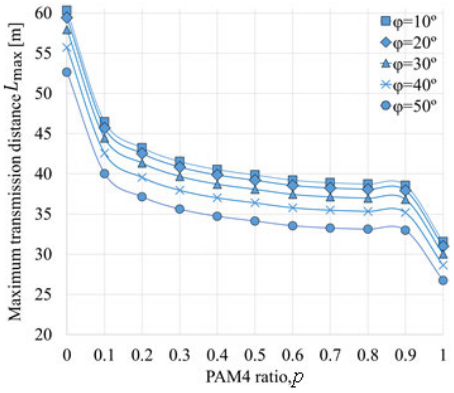

FIGURE 13. Effect of misalignment φ on maximum transmission distance L_{max} for blue LD.

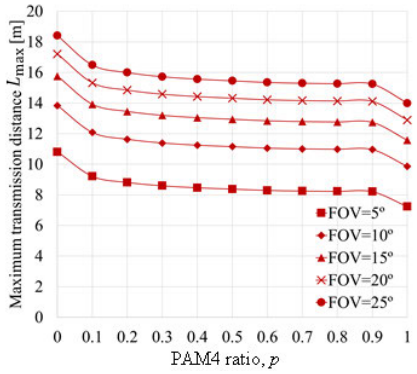

FIGURE 14. Effect of receiver FOV on maximum transmission distance L_{max} for red LD.

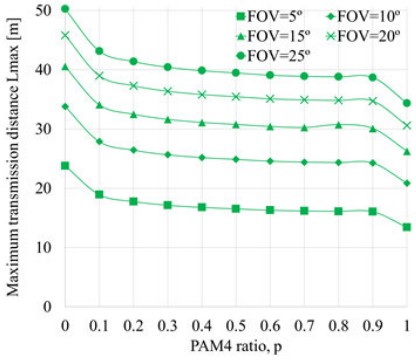

FIGURE 15. Effect of receiver FOV on maximum transmission distance L_{max} for green LD.

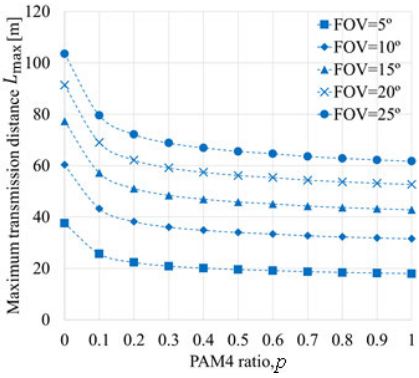

FIGURE 16. Effect of receiver FOV on maximum transmission distance L_{max} for blue LD.

approximately 2.6 m. When the initial value of misalignment $\varphi = 10°$ is used, the green LD L_{max} value is 33 to 20 m. As p increases, L_{max} decreases with the lowest L_{max} value occurring when $\varphi = 50°$ ranging from 18 to 30 m.

Fig. 13 shows the effect of misalignment φ on maximum transmission distance L_{max} using the blue LD. When comparing the L_{max} values for the optimum and non-optimum transmissions, the best improvements occur at approximately 5 m. When the initial misalignment $\varphi = 10°$ is used, the blue LD L_{max} value is 31 to 60 m. As p increases, L_{max} decreases, with the lowest L_{max} value occurring when $\varphi = 50°$ ranging from 27 to 52 m.

From these results, we observe that misalignment φ has little to no effect on L_{max}. As misalignment φ increases, L_{max} decreases by a small amount. Thus, narrowing the misalignment of φ could improve L_{max}, but because the improvement is not significant, we will not consider improving misalignment φ.

C. EFFECT OF FOV

A change in the receiver-side FOV could affect the performance of the receiver for the optimum q value. The FOV of an optical system is the maximum angular size where the PD can receive the optical signals from an LD. A receiver with the same size as the receiver aperture diameter is preferred because it is easier to receive the incoming optical signals even when misalignment occurs.

The effects of the receiver FOV towards L_{max} are evaluated. The L_{max} values range from 5° to 25° in increments of 5° for each measurement. In this simulation, the value of φ is 5°, 10°, 15°, 20°, and 25°.

Fig. 14 shows the effect of the receiver FOV on maximum transmission distance L_{max} using the red LD. When comparing the L_{max} values for the optimum and non-optimum transmissions, the lowest improvements occur at approximately 0.8 m. When the initial receiver FOV = 5° is used, the red LD L_{max} is from 8 to 11 m. As p increases, L_{max} decreases with the highest L_{max} value occurring when receiver FOV = 25° ranging from 14 to 18 m.

Fig. 15 shows the effect of the receiver FOV on maximum transmission distance L_{max} using the green LD. When comparing the L_{max} values for the optimum and non-optimum transmissions, the best improvements occur at approximately 1.7 m. When the initial receiver FOV = 10° is used, the green LD L_{max} value is from 13 to 23 m. As p increases, L_{max} decreases with the highest L_{max} receiver FOV = 25° ranging from 13 to 24 m.

Fig. 16 shows the effect of the receiver FOV on maximum transmission distance L_{max} using the blue LD. When comparing the L_{max} values for the optimum and non-optimum transmissions, the best improvements occur at approximately 6 m.

When the initial receiver FOV = 10° is used, the blue LD $L_{\max}$ value is from 18 to 37 m. As p increases, $L_{\max}$ decreases with the highest $L_{\max}$ value occurring when FOV = 25° ranging from 18 to 37 m.

From these results, we observe that the receiver-side FOV significantly affects $L_{\max}$. As the receiver FOV increases, $L_{\max}$ increases significantly. Widening the receiver-side FOV could improve the performance of $L_{\max}$. As the receiver FOV increases, the easier it is for the receiver to receive the transmitted signal.

VI. CONCLUSION

We concluded that the optimization of the TDHP signal significantly improves the overall performance from the following steps. For selecting the LD, green is chosen because of its optimum wavelength that reduces the absorption/scattering effect of the transmitted signal. Finally, by narrowing half-beamwidth θ and improving the receiver FOV, the overall performance of the UWOC system is improved. When the transmission distance is fixed, the transmission capacity can be increased by changing from PAM 2 to TDHP by reducing θ in the range of $\theta = 10$ to 30 degrees. If the axis deviation increases in the range of $\varphi = 10$ to 50 degrees, it could be dealt with by reducing the p parameter of TDHP and reducing the transmission capacity. If the FOV drops in the range of 5 to 25 degrees during system operation, the p parameter of TDHP can be reduced.

The remaining purpose of testing the performance of UWOC systems in uncontrolled environments such as the sea or dirty water will be considered in future work or applicable scenarios in the next step.

REFERENCES

[1] D. G. Roberson and D. J. Stilwell, "Control of an autonomous underwater vehicle platoon with a switched communication network," in *Proc. Amer. Control Conf.*, vol. 6. Portland, OR, USA, Jun. 2005, pp. 4333–4338.

[2] P. K. Sajmath, R. V. Ravi, and K. K. A. Majeed, "Underwater wireless optical communication systems: A survey," in *Proc. 7th Int. Conf. Smart Struct. Syst. (ICSSS)*, Chennai, India, Jul. 2020, pp. 1–7.

[3] T. Iinuma, R. Hino, N. Uchida, W. Nakamura, M. Kido, Y. Osada, and S. Miura, "Seafloor observations indicate spatial separation of coseismic and postseismic slips in the 2011 Tohoku Earthquake," *Nature Commun.*, vol. 7, no. 1, p. 13506, Dec. 2016.

[4] Y. Inoue, T. Kodama, and T. Kimura, "Global optimization of relay placement for seafloor optical wireless networks," *IEEE Trans. Wireless Commun.*, vol. 20, no. 3, pp. 1801–1815, Mar. 2021.

[5] T. Kodama, K. Arai, K. Nagata, K. Nakamura, and M. Hanawa, "Underwater wireless optical access network with OFDM/SBMA system: Concept and demonstration," in *Proc. 24th Optoelectron. Commun. Conf. (OECC) Int. Conf. Photon. Switching Comput. (PSC)*, Fukuoka, Japan, Jul. 2019, pp. 1–3.

[6] D. Anguita, D. Brizzolara, and G. Parodi, "Building an underwater wireless sensor network based on optical: Communication: Research challenges and current results," in *Proc. 3rd Int. Conf. Sensor Technol. Appl.*, Athens, Glyfada, Jun. 2009, pp. 476–479.

[7] S. Arnon, "Underwater optical wireless communication network," *Opt. Eng.*, vol. 49, no. 1, Jan. 2010, Art. no. 015001.

[8] D. Karunatilaka, F. Zafar, V. Kalavally, and R. Parthiban, "LED based indoor visible light communications: State of the art," *IEEE Commun. Surveys Tuts.*, vol. 17, no. 3, pp. 1649–1678, 3rd Quart., 2015.

[9] J. Sticklus, P. A. Hoeher, and R. Rottgers, "Optical underwater communication: The potential of using converted green LEDs in coastal waters," *IEEE J. Ocean. Eng.*, vol. 44, no. 2, pp. 535–547, Apr. 2019.

[10] T. Kodama, A. Maruta, N. Wada, and G. Cincotti, "Fixed-rate-breaking all-optical OFDM system using time-domain hybrid PAM with sparse subcarrier multiplexing and power-loading for optical short-reach transmission," in *Proc. Opt. Fiber Commun. Conf. Exhib. (OFC)*, San Diego, CA, USA, Mar. 2020, pp. 1–3, Paper T4G.2.

[11] S. Ohlendorf, D. Clausen, R. Rath, S. Pachnicke, and W. Rosenkranz, "Comparison of time domain hybrid PAM and DMT for data center applications," in *Proc. Photonic Netw.; 18. ITG-Symp.* Leipzig, Germany: VDE, May 2017, pp. 1–7.

[12] X. You, J. Chen, Y. Zhong, S. Chen, and C. Yu, "Efficient dimming control with time domain hybrid modulation in indoor hybrid visible Light/Infrared communication systems," in *Proc. 24th Optoelectron. Commun. Conf. (OECC) Int. Conf. Photon. Switching Comput. (PSC)*, Fukuoka, Japan, Jul. 2019, pp. 1–3.

[13] X. You, Z. Liu, J. Chen, M. Gao, C. Yu, and G. Shen, "Location-aware time domain hybrid modulation for mobile visible light communication," in *Proc. Asia Commun. Photon. Conf./Int. Conf. Inf. Photon. Opt. Commun. (ACP/IPOC)*, 2020, p. S4B.

[14] K. Nakamura, K. Nagaoka, D. Matsuo, T. Kodama, and M. Hanawa, "Over 1 Gbit/s NRZ-OOK underwater wireless optical transmission experiment using wideband PMT," in *Proc. 24th Optoelectron. Commun. Conf. (OECC) Int. Conf. Photon. Switching Comput. (PSC)*, Fukuoka, Japan, Jul. 2019, pp. 1–3.

[15] D. Chen, C. Li, and Z. Xu, "Performance evaluation of OOK and PAM modulations in underwater optical wireless communication system based on APD receiver," in *Proc. 16th Int. Conf. Opt. Commun. Netw. (ICOCN)*, Wuzhen, Aug. 2017, pp. 1–3.

[16] T. Kodama, T. Miyazaki, M. Hanawa, A. Maruta, N. Wada, G. Cincotti, and K. Kitayama, "Demonstration of PAM4-OCDM system with electrical amplitude-level pre-tuning and post-equalization for data centers applications," *Opt. Exp.*, vol. 27, no. 8, pp. 11227–11235, 2019.

[17] R. Mesleh, H. Elgala, and H. Haas, "An overview of indoor OFDM/DMT optical wireless communication systems," in *Proc. 7th Int. Symp. Commun. Syst., Netw. Digit. Signal Process. (CSNDSP)*, Newcastle upon Tyne, U.K., Jul. 2010, pp. 566–570.

[18] K. Nakamura, I. Mizukoshi, and M. Hanawa, "Optical wireless transmission of 405 nm, 1.45 Gbit/s optical IM/DD-OFDM signals through a 4.8 m underwater channel," *Opt. Exp.*, vol. 23, no. 2, pp. 1558–1566, 2015.

[19] M. Sui, X. Yu, and F. Zhang, "The evaluation of modulation techniques for underwater wireless optical communications," in *Proc. Int. Conf. Commun. Softw. Netw.*, Feb. 2009, pp. 138–142.

[20] F. Jasman, R. J. Green, and M. S. Leeson, "Impact of receiver field of view on underwater optical wireless communications," *Microw. Opt. Technol. Lett.*, vol. 59, no. 4, pp. 837–840, Apr. 2017.

[21] K. S. Baker and R. C. Smith, "Bio-optical classification and model of natural waters," *Limnol. Oceanogr.*, vol. 27, no. 3, pp. 500–509, 1982.

[22] R. Doerffer and J. Fischer, "Concentrations of chlorophyll, suspended matter, and gelbstoff in case II waters derived from satellite coastal zone color scanner data with inverse modeling methods," *J. Geophys. Res.: Oceans*, vol. 99, no. C4, pp. 7457–7466, 1994.

[23] G. Riccobene *et al.*, "Deep seawater inherent optical properties in the Southern Ionian Sea," *Astropart. Phys.*, vol. 27, no. 1, pp. 1–9, 2007.

[24] R. C. Smith and K. S. Baker, "Optical properties of the clearest natural waters (200–800 nm)," *Appl. Opt.*, vol. 20, no. 2, pp. 177–184, 1981.

[25] S. Matsumoto, Y. Tamura, and K. Nishizawa, "Laser diode and photodiode modules and analogue circuits training for the optical fiber transmission practice system," *Proc. SPIE*, vol. 9665, Jun. 2007, Art. no. 96650X.

[26] V. Mackowiak, J. Peupelmann, Y. Ma, and A. Gorges, *NEP-Noise Equivalent Power*, Thorlabs, Newton, NJ, USA, 2015, vol. 56.

[27] L. F. Suhr, J. J. V. Olmos, and I. T. Monroy, "10-gbps duobinary-4-PAM for high-performance access networks," in *Proc. Asia Commun. Photon. Conf.*, Shanghai, China, 2014, pp. 1–3.

[28] M. Saotome, Y. Kozawa, Y. Umeda, and H. Habuchi, "Differential-OOK system for underwater visible-light communications," *J. Signal Process.*, vol. 20, no. 4, pp. 175–178, 2016.

[29] K. Szczerba, P. Westbergh, J. Karout, J. S. Gustavsson, Å. Haglund, M. Karlsson, P. A. Andrekson, E. Agrell, and A. Larsson, "4-PAM for high-speed short-range optical communications," *IEEE/OSA J. Opt. Commun. Netw.*, vol. 4, no. 11, pp. 885–894, Nov. 2012.

[30] W.-S. Tsai, H.-H. Lu, H.-W. Wu, C.-W. Su, and Y.-C. Huang, "A 30 Gb/s PAM4 underwater wireless laser transmission system with optical beam reducer/expander," *Sci. Rep.*, vol. 9, no. 1, p. 8605, Dec. 2019.

[31] F. P. Guiomar, R. Li, C. R. S. Fludger, A. Carena, and V. Curri, "Hybrid modulation formats enabling elastic fixed-grid optical networks," *J. Opt. Commun. Netw.*, vol. 8, no. 7, p. A92, Jul. 2016.
[32] H. Chun, A. Gomez, C. Quintana, W. Zhang, G. Faulkner, and D. O'Brien, "A wide-area coverage 35 Gb/s visible light communications link for indoor wireless applications," *Sci. Rep.*, vol. 9, p. 4952, Mar. 2019.
[33] J. W. Giles and I. N. Bankman, "Underwater optical communications systems. Part 2: Basic design considerations," in *Proc. IEEE Mil. Commun. Conf. (MILCOM)*, Oct. 2005, pp. 1700–1705.
[34] J. E. Greivenkamp, *Field Guide to Geometrical Optics*. Bellingham, WA, USA: SPIE, 2004.

TAKAHIRO KODAMA (Member, IEEE) received the B.E. degree from Ritsumeikan University, Japan, in 2008, and the M.E. and Dr.Eng. degrees from Osaka University, Osaka, Japan, in 2010 and 2012, respectively.

In 2012, he was selected as a Research Fellow with the Japan Society for the Promotion of Science (JSPS). In 2014, he joined Mitsubishi Electric Corporation, Japan. In 2016, he was a Research Assistant Professor with the Graduate Faculty of Interdisciplinary Research, University of Yamanashi, Japan. Since 2019, he has been a Lecturer with the Faculty of Engineering and Design, Kagawa University. He has published over 90 articles in refereed journals and international conference papers. His research interests include optical access, metro and core networks, optical packet switching networks, digital signal processing, and optical signal processing.

Dr. Kodama is a member of the Institute of Electronics, Information and Communication Engineers (IEICE) of Japan. He was selected as an Excellent Young Researcher of the Ministry of Education, Culture, Sports, Science and Technology (MEXT) of Japan. He was a recipient of the 2011 IEEE Kansai Section Student Paper Award from IEEE.

MUHAMAD AIZAT BIN AHMAD SANUSI received the B.E. degree from Kagawa University, Japan, in 2021.

FUMIYA KOBORI is currently pursuing the bachelor's degree with the Faculty of Engineering and Design, Kagawa University, Japan.

TOMOTAKA KIMURA (Member, IEEE) received the B.Eng., M.Eng., and Dr. Eng. degrees in communications engineering from Osaka University, Japan, in 2008, 2010, and 2015, respectively. From April 2015 to March 2018, he was an Assistant Professor with the Department of Electrical Engineering, Faculty of Engineering, Tokyo University of Science. From April 2018 to March 2020, he was an Assistant Professor with the Department of Intelligent Information Engineering, Faculty of Science and Engineering, Doshisha University, Kyoto, Japan, where he is currently an Associate Professor. His research interests include performance analysis and designs of communication networks. He is a member of IEICE, IEEJ, and JSAI. He received the IEICE Young Researchers Award in 2016.

YOSHIAKI INOUE (Member, IEEE) was born in Hyogo, Japan, in 1989. He received the B.Eng., M.Eng., and Dr. Eng. degrees in communications engineering from Osaka University, Osaka, Japan, in 2011, 2013, and 2016, respectively. He was with the Eindhoven University of Technology, Netherlands, as a Visiting Researcher, from May 2015 to November 2015. He is currently an Assistant Professor with the Department of Information and Communication Technology, Graduate School of Engineering, Osaka University. His research interests include queuing theory and performance evaluations of information and communications systems. He is a member of ORSJ and IEICE.

MASAHIKO JINNO (Fellow, IEEE) received the B.E. and M.E. degrees in electronics engineering from Kanazawa University, Japan, in 1984 and 1986, respectively, and the Ph.D. degree in engineering from Osaka University, Osaka, Japan, in 1995, for his work on ultra-fast optical signal processing based on nonlinear effects in optical fibers. He is currently working as a Professor with the Faculty of Engineering and Design, Kagawa University, Takamatsu, Japan. Prior to joining Kagawa University in October 2012, he was a Senior Research Engineer and a Supervisor with Nippon Telegraph and Telephone (NTT) Network Innovation Laboratories, NTT Corporation conducting pioneering research on spectrum- and energy-efficient elastic optical networks (EONs). From 1993 to 1994, he was a Guest Scientist with the National Institute of Standards and Technology, Boulder, CO, USA. He has authored or coauthored more than 180 peer-reviewed journal and conference papers in the fields of ultra-fast optical signal processing for high-capacity optical time division multiplexed transmission systems, optical sampling and optical time-domain reflectometer, ultra-wideband DWDM transmission systems in the L-band and S-band, ROADM systems, GMPLS and application-aware optical networking, EONs, and SDM networks. His current research interests include architecture, design, management, and control of optical networks, optical transmission systems, optical cross-connects, optical switches, and rate- and format-flexible optical transponders. He is a fellow of the Institute of Electronics, Information and Communication Engineers (IEICE) and a member of the Optical Society of America. He received the Young Engineer's Award, in 1993, the Best Tutorial Paper Award, in 2011, the Best Paper Award, in 2012, the Achievement Award, in 2017, and the Milestone Certificate from the IEICE, in 2017, the Best Paper Awards from the 1997, 1998, 2007, and 2019 Optoelectronics and Communications Conferences, the Best Paper Award from the 2010 ITU-T Kaleidoscope Academic Conference, and the Outstanding Paper Award from the IEEE Communications Society Asia-Pacific Board, in 2013.